Solar Activation of TiO2 Intensified with Graphene for Degradation of Bisphenol-A in Water

Solar Activation of TiO_2 Intensified with Graphene for Degradation of Bisphenol-A in Water

J.M. Monteagudo[a]*, A. Durán[a], E. Chatzisymeon[b], I. San Martín[a], S. Naranjo[a]

[a] *Department of Chemical Engineering, Grupo IMAES, Escuela Técnica Superior de Ingenieros Industriales, Instituto de Investigaciones Energéticas y Aplicaciones Industriales (INEI)University of Castilla-La Mancha, Avda. Camilo José Cela 3, 13071 Ciudad Real (Spain).*

[b] *Institute for Infrastructure and Environment, School of Engineering, The University of Edinburgh, Edinburgh EH9 3JL, United Kingdom.*

* To whom correspondence should be addressed

Department of Chemical Engineering, Grupo IMAES
Escuela Técnica Superior de Ingenieros Industriales,
Instituto de Investigaciones Energéticas y Aplicaciones Industriales (INEI)
University of Castilla-La Mancha,
Avda. Camilo José Cela 3, 13071 Ciudad Real (Spain).
Fax: 0034 926295361.
Phone: 0034 926295300, ext: 3888
Email: josemaria.monteagudo@uclm.es

ABSTRACT

Photocatalytic degradation of a Bisphenol-A (BPA) aqueous solution was achieved using titanium dioxide (TiO_2) and graphene-based TiO_2 photocatalysts activated by solar light. First, a comparative study of the adsorption kinetics of BPA, in the presence of both catalysts, as a function of pH was performed. Then, the effect of the initial BPA concentration and catalyst loading was assessed and the optimal conditions for BPA degradation by means of heterogeneous solar photocatalysis were determined. It was observed that TiO_2 modified with 2 wt% graphene improved the photocatalytic efficiency in terms of BPA mineralization. The TiO_2/graphene photocatalytic composite achieved a 16% increase in the photocatalytic mineralization of the BPA solution under solar light compared to un-doped TiO_2. This enhancement of photocatalytic efficiency is a result of the increase of active sites for BPA adsorption, the more efficient harvesting of solar light, and the inhibition of electron-hole recombination. The dynamic behavior of hydroxyl radicals and dissolved oxygen in these systems was also discussed. Finally, the roles played by hydroxyl radical, $HO^{\bullet}$, superoxide radical anion, $O_2^{\bullet-}$, and singlet molecular oxygen, $^1O_2$, were studied in both TiO_2 and TiO_2/graphene systems. It was found that $O_2^{\bullet-}$ were the main oxidative species in both systems.

Keywords: bisphenol-A; TiO_2/graphene; oxidative species; solar light.

1. INTRODUCTION

Bisphenol-A (BPA) is a well-known endocrine disrupting chemical (EDC) that has been extensively detected in the environment. BPA can cause adverse health effects due to its interference with the human and animal hormones (Schafer et al., 1999; Gultekin et al., 2009; Rubin, 2011; Rogers et al., 2013). Due to its xenobiotic nature, this molecule cannot be completely degraded by the biological treatment processes used in wastewater treatment plants (WWTPs) and it is therefore discharged intact into the environment (Hu et al., 2007; Crain et al., 2007). Hence, an efficient treatment system for removing BPA or its oxidation reaction intermediates from the aquatic environment remains a pressing need for water industry and decision makers.

It is well-known that Advanced Oxidation Processes (AOPs) are effective methods for treating organic pollutants in water. The efficacy of AOPs is based on the generation of highly reactive free radicals, especially hydroxyl radicals ($HO^{\bullet}$) or sulfate radicals ($SO_4^{\bullet-}$), which are capable of transforming bio-recalcitrant molecules into biodegradable products. Among AOPs, heterogeneous photocatalytic degradation reactions using semiconductor metallic oxides, such as TiO_2, as photocatalysts to destruct persistent organic pollutants such as EDCs have been well studied (Esplugas et al., 2007; Durán et al., 2009; Xekoukoulotakis et al., 2011). Reactive oxygen species, mainly hydroxyl radical, superoxide radical anion, $O_2^{\bullet-}$, and singlet molecular oxygen, $^1O_2$, which can degrade a wide range of chemical contaminants in water, are generated during photocatalytic processes. However, the production of photons by means of artificial light sources requires a substantial amount of electrical energy (Pérez et al., 2002). Solar energy can be used, alternatively to UV lamps, as a more sustainable option in order to reduce the energy and costs of the water treatment process. TiO_2-assisted photocatalytic

89 degradation of several organic contaminants by solar light has been successfully used.
90 This was found to be an economically viable process since solar energy is an abundant
91 natural energy source and can be used instead of artificial light sources which are costly
92 and hazardous (Konstantinou and Albanis, 2003; Robert et al., 2004). TiO_2 has a wide
93 band gap (anatase E_{bg}= 3.2 eV or $\lambda < 387$ nm) and requires UV excitation (energy equal
94 to or greater than the band-gap) to form electron-hole pairs. The conduction band
95 electrons are able to reduce dissolved oxygen to generate superoxide radical, $O_2^{\bullet-}$,
96 hydroperoxyl radicals, $HO_2^{\bullet}$, and through subsequent reduction reactions, hydrogen
97 peroxide, H_2O_2, and hydroxyl radical, $HO^{\bullet}$. The valence band holes, h^+, are able to
98 oxidize water to form $HO^{\bullet}$. The drawbacks of solar photocatalysis are that the UV
99 radiation received by the earth is only around 5% of the entire solar energy spectrum
100 and the photogenerated electron-hole pairs have fast recombination rates. In this sense,
101 the efficiency of solar photocatalysis can be improved by doping TiO_2 composites with
102 materials, such as graphene (Kumordzi et al., 2016), in order to expand the catalyst
103 band-gap to the visible light region of the solar spectrum ($\lambda > 400$ nm) and prevent
104 electron-hole pair recombination (Fukahori et al., 2003; Bellobono et al., 2005; Ni et al.,
105 2007; Fujishima et al., 2008). The use of graphene is of great scientific interest due to
106 its excellent properties such as chemical inertness, stability in both acidic and basic
107 mediums, its abundance and large surface area (2630 m^2/g) (Upadhyay et al., 2014).
108
109 BPA degradation has been previously investigated in many oxidative treatment
110 processes, such as UV/H_2O_2 and UV/persulfate (Yoon et al., 2012). A comparative
111 study on the oxidative degradation of BPA by Fenton reagent, UV, UV/H_2O_2 and
112 Ultrasound has been also reported (Young et al., 2013). The removal of BPA by means
113 of UV, UV/H_2O_2, UV/$K_2S_2O_8$ and UV/Na_2CO_3 processes was also studied (Sánchez-

Polo et al., 2013). F–TiO_2–RGO nanocomposites were examined for BPA degradation under UV light illumination (Luoa et al., 2015). TiO_2/graphene/Cu_2O was applied in the photoelectrocatalytic oxidation of BPA under artificial visible light irradiation (Yanga et al., 2016). The catalytic ability of TiO_2–reduced graphene oxide hybrid (TiO_2 – RGO) in photocatalysis using an artificial 365 nm light and ozonation combined system to degrade BPA was also investigated (Liao et al., 2016).

However, to the best of our knowledge, the application of graphene-TiO_2 composites irradiated by natural solar light for BPA degradation has not been studied yet. Therefore, further studies are required in this area to develop a more sustainable and cost efficient treatment technology. The aim of this work is to investigate BPA mineralization reactions by using solar photocatalytic oxidation in the presence of TiO_2 and TiO_2/graphene composites. First, the influence of pH on BPA adsorption kinetics for both TiO_2 and TiO_2/graphene composites was investigated. Then, the effects of various process parameters, such as initial concentrations of BPA and suspended photocatalysts as well as the type of the catalyst on mineralization reactions were evaluated. Afterwards, the dynamic behavior of $HO^{\bullet}$ radicals and the profile of dissolved oxygen in both catalytic systems were determined. Finally, the roles played by different reactive oxidative species such as $HO^{\bullet}$, $O_2^{\bullet-}$ and $^1O_2$, in both TiO_2 and TiO_2/graphene systems were evaluated using appropriate scavengers.

2. EXPERIMENTAL

2.1. Materials

BPA (CAS No: 80-05-7) (Fig. 1a), p-benzoquinone, sodium azide and ethanol (99.5%) were purchased from Sigma-Aldrich. Aeroxide® TiO_2 P25 was supplied by Evonik Industries and graphite powder (natural, microcrystal grade, product no. 14736) was purchased from Alfa Aesar. Tert-butyl alcohol was purchased from Panreac. All chemicals were used as received without further purification. The pH of the wastewater in each test was adjusted using H_2SO_4 and NaOH solutions.

2.2. Photocatalyst preparation and characterization

Graphite oxide, GO, was obtained from graphite powder through the modified Hummers method (Hummers and Offeman, 1958; Hassan et al., 2013). GO was dissolved in a water/ethanol (2:1) solution followed by 60 min ultrasound treatment. Then, a calculated amount (to obtain concentrations of 1, 2 and 3 wt% of graphene) of commercial TiO_2 nanoparticles (P25) was added to the GO solution, which was continuously stirred for 3 h. The mixture was transferred to a Teflon-lined autoclave, and the hydrothermal process was performed at 120 ºC for 15 h. During this process, GO could be reduced to graphene and the deposition of TiO_2 was achieved. Then, the obtained composites were centrifuged, rinsed with deionized water, and dried at 60ºC. The prepared samples are denoted as TiO_2/graphene.

Structural analyses of TiO_2 and TiO_2/graphene samples were determined by X-ray Diffraction (XRD) using a PHILIPS X'Pert MPD PW 3040 analyzer with a Cu KAlpha1 radiation. Ultraviolet-visible (UV-Vis) spectra were collected in a Cary 100 diffuse reflectance UV-Vis spectrophotometer. Transmission electron microscopy

(TEM) images were obtained using a JEOL JEM-2100Plus microscope. The specific surface area, pore size and pore volume of the samples was measured with Brunauer-Emmett-Teller (BET) method using the Micro-meritics Gemini VII 2390 by using N_2 adsorption at 77 K.

2.3. Experimental set-up

Fig. 1b illustrates the scheme of the experimental set-up. A CPC solar reactor with a surface of 0.25 m^2, manufactured by Ecosystem, S.A., consisted of 2 borosilicate tubes and an irradiated volume of 2 L. The reactor was mounted on a fixed south-facing platform tilted 39º in Ciudad Real (Spain). It included a continuously stirred tank (volume= 1.5 L) and a centrifugal recirculation pump (flow rate: 30 L min^{-1}).

2.4. Adsorption studies

To analyze BPA adsorption on TiO_2 or TiO_2/graphene composites, different experiments were conducted in the dark using the experimental reactor indicated above. 3.5 L of aqueous solution containing 10 mg L^{-1} BPA solution were prepared by weighing and dissolving, by ultrasound mixing for 3 hours, the appropriate amount of BPA in deionized water. Then, the appropriate amount of catalyst (TiO_2 alone or TiO_2/graphene) was added to the solution to reach a concentration of 125 mg L^{-1} TiO_2. Solution pH can affect both the adsorbent electrical surface charge and the dissociation of the adsorbate. The effect of pH on adsorption of BPA by TiO_2 or by TiO_2/graphene was studied fixing the initial pH value of the solutions at 7.5 and 2.5. These pH values

were chosen taking into account the point of the zero charge (PZC) of TiO_2 (between pH= 5.6 and 6.4 (Daneshvar et al., 2004). It is well-known that the surface charge of TiO_2 depends on pH. At more acidic pH values, the TiO_2 surface is positively charged and above TiO_2 PZC, the surface is negatively charged.

Samples were agitated at room temperature for a period of 2 h before being filtered through 0.45 μm syringe filters to separate catalyst particles and to analyze the residual concentrations of BPA.

2.5. Solar photocatalytic process

In a typical solar TiO_2 or TiO_2/graphene photocatalytic run, BPA was dissolved in deionized water as indicated above. This BPA solution was then transferred into a reservoir and the appropriate pre-weighted amount of TiO_2 or TiO_2/graphene catalyst was added in it. The BPA solution was stirred in the dark for 30 minutes to attain adsorption equilibrium between BPA and catalyst particles. The reactant mixture was then pumped through the CPC and solar photocatalytic oxidation started. During the experiments, samples were periodically withdrawn from the reactor and filtered through 0.45 μm syringe filters to separate catalyst particles from the liquid. Chemical analyses for BPA, $HO^{\bullet}$, Total Organic Carbon (TOC) and dissolved oxygen content were performed.

To quantify the oxidation levels by $HO^{\bullet}$, $O_2^{\bullet-}$ and $^1O_2$, 1 M tert-butyl alcohol, 2 mM 1,4-benzoquinone and 2 mM sodium azide were used as scavenging agents, respectively.

All experiments were performed in triplicate, and the medium values were used. Before analysis, all filtered samples were immediately treated with excess Na_2SO_3 to prevent further oxidation (this procedure was performed to avoid overestimating degradation). All the experiments were conducted at room temperature and at natural pH of BPA solution (≅ 7.5).

2.6. Analysis

BPA concentration was determined using high-performance liquid chromatography with UV detection (Agilent Technologies 1100 HPLC-UV) in the isocratic mode immediately after sampling. An Eclipse XDB-C18 column (5 mm, 4.6 × 250 mm) was used, and a 75:25 (v/v) methanol/(water with 1% acetic acid) mixture with an acidic pH was used as the mobile phase (detection wavelength, λ= 225 nm; flow rate of 0.6 ml min^{-1}). The mineralization grade of the treated wastewater was determined using a TOC analyzer (TOC-5050 Shimadzu, standard deviation < 0.2 mg L^{-1}). Quantification of hydroxyl radicals was carried out by fluorescence measurement using disodium salt of terephthalic acid (NaTA) (Saran and Summer, 1999). Dissolved oxygen concentration was measured using a Jenway 9200 DO_2 meter.

3. RESULTS AND DISCUSSION

3.1. Characterization Results

Surface area and porosity measurement

The specific surface area, pore volume, and the pore size of the samples are summarized in Table 1. The BET surface area of the TiO_2 increased (10 %) with graphene incorporation, indicating that the physical adsorptivity of the nanocomposite was improved. This is presumably due to the high theoretical specific surface area (2600 m^2/g) of reduced graphene oxide (Akhavan and Ghaderi, 2009). The pore size distribution was also estimated using the Barrett-Joyner-Halenda (BJH) method (Lellala et al., 2016) from the desorption branch of the isotherm. It can be seen that compared to the pure TiO_2, the pore volume of TiO_2/graphene was increased, which is vital to improve the adsorption capacity of the nanocomposite and to increase the efficiency of separation of electron-hole pairs (Saha et al., 2012). In addition, the values showed average pore diameter characteristic of mesoporous materials, which is important for photocatalytic applications.

UV-Vis diffusive reflectance spectroscopy

The TiO_2 absorption capacity can be studied by UV-Vis diffusive reflectance spectroscopy. Fig. 2 shows that both pure TiO_2 and TiO_2/graphene have high absorption capacities in the UV region. However, only TiO_2/graphene composite exhibited a broad adsorption spectra in the visible region. That shows the possibility of visible light photocatalyst by TiO_2/graphene composite.

X-Ray diffraction (XRD)

X-Ray diffraction (XRD) was used to examine the crystalline structure of TiO_2 and TiO_2/graphene 2 wt%. Figs. 3a and 3b show XRD patterns obtained for TiO_2 and TiO_2/graphene, respectively. As it is shown, TiO_2/graphene exhibited a similar XRD pattern to pure TiO_2. Anatase and rutile crystalline phases were observed in both composites. Peaks associated only with TiO_2 were observed and no peak was assigned to GO. This indicates that GO was reduced to graphene during the hydrothermal treatment. Graphene did not affect the crystalline structure of TiO_2. The XRD patterns of the samples revealed the crystalline structure of the anatase TiO_2 phase due to the presence of a distinct diffraction peak at 2θ of 25.2° that correspond to the {011} crystal plane. This peak and their corresponding reflections agree with ICSD collection code nº 96946 for anatase. The peak diffraction of the rutile TiO_2 phase was observed at 2θ of 27.4° corresponding to the {110} crystal plane (ICSD collection code nº 76172). The proportion anatase: rutile and the maximum intensities of the peaks of anatase and rutile phases in the diffractograms were almost the same in both samples (anatase: rutile: 87:13 for TiO_2 and 86:14 for TiO_2/graphene; maximum intensities: 509 and 76 counts, respectively, for TiO_2 and 524 and 87 counts, respectively, for TiO_2/graphene). It is well known that the intensity of the diffracted peak from a given crystalline structure of the element (i.e., anatase or rutile phase) is proportional to the amount of the structural element present in the crystal sample. The TiO_2 modified with graphene did not suffer modifications in its crystalline structure. It is well-known that anatase form has a photocatalytic activity greater than rutile (Wang and Yu, 2013) which indicates that anatase can generate more oxidative species than rutile and besides the recombination rate of holes and electrons is lower in the anatase phase than in the rutile phase.

Figs. 3c-f present the TEM images of TiO_2/graphene-2 wt% nanocomposite. It can be seen clearly the spherical TiO_2 nanoparticles and the graphene oxide sheets, which is covered with TiO_2 nanoparticles. Intraparticle aggregation formed a mesoporous structure, which was previously confirmed by nitrogen adsorption−desorption analysis. The average diameter of TiO_2 nanoparticles was about 10–30 nm, which is in agreement with the mean crystal size value of 19 nm estimated by the Scherrer equation (Patterson, 1939) based on (200) peak from the X-ray diffractogram.

3.2 Bisphenol-A adsorption kinetics

TiO_2 and TiO_2/graphene particles consist of different adsorption sites which will define the adsorption ability of each catalyst. Two models were tested to analyze BPA adsorption: a) Lagergren model, a pseudo-first-order adsorption rate equation (Lagergren, 1898) and b) Ho and McKay model, pseudo-second-order adsorption rate equation (Ho and McKay, 1999).

The Lagergren equation can be represented by the following equation:

$$\frac{dQ_t}{dt} = k_1(Q_e - Q_t) \quad (1)$$

where Q_e and Q_t are the values of BPA mass adsorbed per unit mass of adsorbent at equilibrium and time t (mg g^{-1}), respectively, and k_1 is the pseudo-first-order rate constant (min^{-1}). The integration of Eq (1) gives the following equation:

$$\log(Q_e - Q_t) = \log(Q_e) - \frac{k_1}{2.303}t \quad (2)$$

Plot of *log* $(Q_e\text{-}Q_t)$ versus *t* would yield a straight line if the adsorption follows a pseudo-first order kinetic behaviour. This model is based on the assumption that the adsorption rate depends on the number of adsorption sites on the adsorbent surface (Lagergren, 1898). Figs. 4a and 4b show the kinetics of adsorption of BPA on the TiO_2 and TiO_2/graphene surface, respectively, at both pH values, 2.5 and 7.5. We can see that the pseudo-first-order kinetics for both systems, TiO_2 and TiO_2/graphene, was found to be suitable only for an initial interaction time (up to 60 min) and not for the 120 min of total contact time.

The pseudo-second order kinetic model (Ho and McKay model), given by Eq (3) is based on the assumption that the adsorption rate is determined by the square of the number of vacant adsorption sites on the adsorbent surface (Ho and McKay, 1999).

$$\frac{dQ_t}{dt} = k_2(Q_e - Q_t)^2 \quad (3)$$

where Q_e and Q_t are the values of BPA mass adsorbed per unit mass of adsorbent at equilibrium and time *t* (mg g^{-1}), respectively, and k_2 is the pseudo-second-order rate constant (g min^{-1} mg^{-1}). The integration of Eq (3) gives the following expression:

$$\frac{t}{Q_t} = \frac{1}{k_2(Q_e)^2} + \frac{1}{Q_e}t \quad (4)$$

Figs. 4c and 4d show the plot of t/Q_t versus t for the adsorption of BPA by TiO_2 and TiO_2/graphene catalysts, respectively, for the two studied pH values, 2.5 and 7.5. As it can be seen, the data fit well to a pseudo-second-order rate kinetics at both pH values for the whole contact time. As shown in Table 2, it can be concluded that: (i) the k_2 values are higher for BPA adsorption on TiO_2/graphene than in pure TiO_2; (ii) in both systems, k_2 values depend on the medium pH being higher at pH 7.5 since it takes a shorter time to reach equilibrium (values of $k_2(BPA\text{-}TiO_2)$= 0.0007 and 0.0037 g min^{-1} mg^{-1} at pH 2.5 and 7.5, respectively, and k_2(BPA-TiO_2/graphene)= 0.0029 and 0.0043 g min^{-1} mg^{-1} at pH 2.5 and 7.5, respectively. This may be explained by the abatement of hydrogen ions after the increase of pH, which reduces the chance of competition between hydrogen ions and the BPA molecules. Due to the natural negative charge of TiO_2 at pH > PZC and the natural negative charge of GO over this whole pH range, it would be possible for hydrogen ions to be adsorbed by TiO_2 and TiO_2/graphene through electrostatic interactions. On the other hand, at pH < 4.5, catalyst particles agglomeration could reduce the BPA adsorption as well as photon absorption (Muruganandham and Swaminathan, 2004); (iii) the adsorption capacity, Q_e, of BPA by TiO_2/graphene catalyst is higher than that by pure TiO_2 being approximately 31 and 18 mg g^{-1}, respectively.

When adsorption data follow a pseudo-second-order kinetics, the rate limiting step may be chemical adsorption. The excellent adsorption ability may be attributed to π-π stacking interaction and hydrogen bond between BPA and graphene in agreement with other authors (Shen et al., 2014; Jin et al., 2015). Taking into account these adsorption

results and the natural pH of BPA solution (≅7.5), this value of pH was chosen as optimal pH for all the photocatalytic experiments.

.

3.3 Degradation of BPA by solar TiO_2 process

The degradation reaction of BPA solutions using a solar/TiO_2 photocatalytic system was investigated to find out the optimal values for the initial concentrations of BPA and TiO_2 being 2.5 mg L^{-1} and 250 mg L^{-1} the selected values, respectively (Figs. S1-S4, Supplementary Material).

3.4 Degradation of Bisphenol-A by solar graphene-based TiO_2 process

To evaluate the performance of the catalytic activity of the TiO_2/graphene catalyst, the degradation of 2.5 mg L^{-1} BPA aqueous solution using 250 mg L^{-1} TiO_2/graphene catalyst (1, 2 and 3 wt% graphene concentrations with respect to TiO_2) under natural solar light was tested. The initial pH was 7.5 in all experiments. The solar power was around 25-30 W/m^2, and the average temperature was around 26ºC in all experiments. Fig. 5a shows an enhancement in the mineralization efficacy of the BPA solution with the TiO_2/graphene catalyst compared to TiO_2 alone. The percentage of TOC removal increased when TiO_2 was modified with amounts of graphene up to 2 wt%. Fig. 5b exhibits that the incorporation of graphene enhances their photoactivity for BPA mineralization. As can be observed, as the weight percentage of graphene increased from 0 to 2% at a fixed catalyst concentration of TiO_2 (250 mg L^{-1}) the pseudo-first-order kinetic rate constant increased from 0.0128 to 0.0149 min^{-1}, respectively, which

374 indicates about 16% improvement over that of pure TiO_2 catalyst. This improvement on
375 the performance of TiO_2/graphene could be due to the following: (a) the increase of
376 catalytic surface active sites for the adsorption of BPA, as was discussed in the previous
377 section, resulting in a more efficient photocatalytic process, (b) a good assembly and
378 interfacial coupling between TiO_2 and graphene sheets, as observed by TEM images
379 (Figs. 3c-f), could promote charge migration between both phases and increase the
380 catalyst efficiency, (c) graphene when combined with TiO_2 reduced charge
381 recombination, facilitating the electron-hole separation and the availability of photo-
382 generated e^- for the photocatalytic reaction, and (d) the introduction of graphene
383 allowed a more efficient utilization of the solar spectrum (Malekshoar et al., 2014). It
384 may note that when 3 wt% of graphene was used, the mineralization efficiency was
385 lower possibly because the photoactivity of the catalyst decreased due to an increase in
386 catalyst agglomerate size and a decrease in light penetration.

387

388 *3.5 $HO^\bullet$ and dissolved O_2 behavior in solar/TiO_2 and solar/TiO_2/graphene*

389

390 Figs. 6a and 6b show the behavior of hydroxyl radical and dissolved oxygen,
391 respectively, along BPA degradation reactions by means of the solar/TiO_2 process and
392 for different initial concentrations of the organic pollutant. The initial concentration of
393 BPA varied between 2.5 and 10 mg L^{-1} in the presence of 125 mg L^{-1} TiO_2. The solar
394 power in these experiments was around 25-30 W/m^2, and the average temperature was
395 26ºC. The reaction time was 120 min in all experiments. As it can be seen, when an
396 initial concentration of BPA below 5 mg L^{-1} was used, the concentration of $HO^\bullet$ rapidly
397 increased reaching a maximum value at around 6-10 min and then it remained constant.

Above 5 mg L^{-1} BPA, the increase of the hydroxyl concentration was much lower reaching values of approximately 2000 and 500 nmol L^{-1} for 7.5 and 10 mg L^{-1} BPA, respectively. The greater concentration of $HO^{\bullet}$ (≅ 13500 nmol L^{-1}) was obtained using the smaller concentration of BPA, 2.5 mg L^{-1}, being higher both the BPA and TOC removal in this case due to the higher TiO_2 photocatalytic efficiency, as indicated above.

Fig. 6b shows measurements of dissolved oxygen concentration during the solar/TiO_2 process at different initial BPA concentrations. It can be observed that the behaviour of dissolved oxygen was similar in all experiments although its concentration was lower when the initial BPA concentration was increased. In the first reaction stage, dissolved oxygen was decreased by reacting with the photo-excited electrons in the conduction band (Eq. (5)), thus generating superoxide radical anion, $O_2^{\bullet-}$. During this time period, solution TOC decreased (see Fig. S2, Supplementary Material). In a second reaction phase, after 90 min, when TOC remained constant, possibly due to the formation of recalcitrant intermediates, hard to be degraded, the concentration of dissolved O_2 was slightly increased according to reactions (6)-(8).

$$O_2 + e_{CB}^- \rightarrow O_2^{\bullet-} \quad (5)$$

$$O_2^{\bullet-} + H^+ \leftrightarrow HO_2^{\bullet} \quad (6)$$

$$2HO_2^{\bullet} \rightarrow O_2 + H_2O_2 \quad (7)$$

421

422 $$H_2O + 4h^+ \rightarrow \frac{1}{2}O_2 + 2H^+ \quad (8)$$

423

424 Figs. 6c and 6d show the behavior of hydroxyl radical and dissolved oxygen during
425 BPA treatment by the solar/TiO_2 process in the presence of different initial TiO_2
426 concentrations of TiO_2 (between 100 and 500 mg L^{-1}). For the sake of comparison,
427 results during BPA treatment by means of the solar/TiO_2/graphene (250 mg L^{-1}
428 TiO_2/2wt% of graphene) system are also shown in these figures. The initial
429 concentration of BPA was fixed at 5 mg L^{-1}. The solar power in these experiments was
430 around 25-30 W/m^2, and the average temperature was 26ºC. The reaction time was 120
431 min in all experiments. It can be seen that, in the solar/TiO_2 process, the increase of
432 TiO_2 loading from 100 to 250 mg L^{-1} led to the increase in $HO^{\bullet}$ generation due to the
433 increase of active sites on the catalyst surface and consequently to the increase in the
434 photocatalytic yield and percentage of BPA and TOC removal, as indicated above. It
435 can be also seen the reduction in the production of $HO^{\bullet}$ when the initial concentration of
436 TiO_2 was 500 mg L^{-1}, justifying the degradation results indicated above. Also, Fig. 6c
437 shows the behavior of $HO^{\bullet}$ when TiO_2/graphene (250 mg L^{-1} TiO_2 with 2 wt% of
438 graphene) irradiated by solar light was used. In this case, the concentration of $HO^{\bullet}$
439 showed a similar tendency and it was slightly higher than under the same conditions in
440 the presence of pure TiO_2 catalyst. This could be attributed to the consumption of $HO^{\bullet}$
441 by reaction with superoxide radical, $O_2^{\bullet-}$, to form singlet molecular oxygen, in the
442 solar/TiO_2 process as given in Eq. (9):

443

444 $$O_2^{\bullet-} + HO^{\bullet} \rightarrow {}^1O_2 + OH^- \quad (9)$$

With respect to the dissolved oxygen, Fig. 6d showed a similar behavior of O_2 in the BPA solution although its values were slightly higher when the initial TiO_2 loading increased in the solar/TiO_2 treatment process. This could be attributed to higher rates of recombination of electrons and holes, which decreased the availability of photogenerated electrons, e^-_{CB}, to react with oxygen. However, as can be also seen in Fig. 6d, when TiO_2 was modified with graphene (250 mg L^{-1} TiO_2 and 2 wt% of graphene) a more pronounced decrease of dissolved oxygen was observed, possibly due to a higher amount of e^-_{CB} on the catalyst surface which consumed more O_2 forming superoxide radical and therefore inhibiting the hole/electron recombination. Thus, the photocatalytic efficacy was higher in the solar TiO_2/graphene treatment process as indicated above.

3.5 Role of different oxidative intermediate species

The contributions of various oxidative intermediate species to the degradation of BPA using both solar/TiO_2 and solar/TiO_2/graphene processes were also examined. To quantify the oxidation levels by free radical reactions, the scavenging of intermediate active species was accomplished with 1 M concentration of tert-butyl alcohol ($HO^\bullet$ and $HO_2^\bullet$ quencher), 2 mM 1,4-benzoquinone ($O_2^{\bullet-}$ quencher) and 2mM sodium azide ($^1O_2$ quencher) (Li et al., 2009; Monteagudo et al., 2011). Several additional experiments under solar/TiO_2 and solar/TiO_2/graphene process were carried out at the optimal conditions in the presence or absence of these scavengers. In these reactions, various oxidative intermediate species could be generated, such as the hydroxyl radical ($HO^\bullet$),

hydroperoxyl ($HO_2^{\bullet}$), singlet oxygen ($^1O_2$), and the superoxide radical anion ($O_2^{\bullet-}$). The roles of these species are shown in Figs. 7a and 7b. As shown, the presence of some scavenging agents inhibited the degradation reaction (the %BPA removal decreased as compared with the scavenger-free reaction). This indicates the participation of these species in the reaction. Superoxide radical anion, $O_2^{\bullet-}$, was found to be the primary species contributing to the degradation of BPA in both solar/TiO_2 and solar/TiO_2/graphene systems since p-benzoquinone was the most significant scavenging agent. In the case of TiO_2/graphene treatment system, this may be due to the formation of a heterojunction interface in the TiO_2/graphene composites, where there is a space-charge separation region, graphene nanosheets can accept photogenerated electrons from the TiO_2 conduction band. This reduced the electron-hole pair recombination, and subsequently the oxygen molecules adsorbed on the catalyst surface act as electron scavengers and combine with e^-_{CB} to form $O_2^{\bullet-}$, according to reaction (5) indicated above. $O_2^{\bullet-}$ is in an acid-base equilibrium (Eq. (6)) but these species predominated over $HO_2^{\bullet}$ since the medium pH was around 7 (pKa ($HO_2^{\bullet}$) = 4.8 ±0.1) (Bielski et al., 1985).

From Fig. 7, it can be also concluded that singlet molecular oxygen, $^1O_2$, played a role in the degradation of BPA, but it was more significant in the pure TiO_2 rather than in the TiO_2/graphene treatment system. $^1O_2$ is formed by $O_2^{\bullet-}$ oxidation by holes, h^+, according to Eq. (10):

$$^{\bullet}O_2^- + h^+ \rightarrow {}^1O_2 \qquad (10)$$

In the case of solar/TiO_2 treatment reaction, the role played by hydroxyl radical, $HO^{\bullet}$, was less significant than that played by singlet oxygen. This could be attributed to the participation of $HO^{\bullet}$ radicals instead of h^+ in Eq. (10) as given in Eq (9) (Daimon et al.,

493 2008), thus decreasing the availability of hydroxyl radicals for the degradation reaction.
494 However, the role of $HO^{\bullet}$ was more significant than that played by $^1O_2$ in the
495 degradation of BPA under the solar TiO_2/graphene process possibly due to the higher
496 availability of h^+ as indicated above. In this case, the contribution of $HO^{\bullet}$ to the $^1O_2$
497 formation was less significant in comparison with the oxidation by h^+.

498

499 **4. Conclusions**

500

501 The solar photocatalytic degradation and mineralization of a BPA aqueous solution in
502 the presence of TiO_2/graphene composites was compared to that of pure TiO_2
503 photocatalyst. The TiO_2/graphene catalyst was prepared by a simple hydrothermal
504 treatment method. The results showed that there was an improvement in both the
505 reaction rate and the mineralization degree when TiO_2 was modified with graphene.
506 This higher efficiency could be attributed to the increase of the active sites for
507 adsorption of BPA, to the more effective use of solar spectrum, to the inhibition of
508 electron-hole recombination and the increase of catalyst efficiency by the charge
509 migration between TiO_2 and graphene. Experimental results showed that 20 and 120
510 min of 25-30 W m^{-2} solar irradiation were required to degrade 2.5 mg L^{-1} Bisphenol-A
511 and 84% solution TOC, respectively, when 250 mg L^{-1} TiO_2/graphene-2 wt% was used.
512 Superoxide radical, $O_2^{\bullet-}$, was found to be the primary species contributing to the
513 degradation of BPA in both solar/TiO_2 and solar/TiO_2/graphene systems. In the case of
514 solar/TiO_2 reaction, hydroxyl radicals, $HO^{\bullet}$, played a less important role than that of
515 singlet oxygen, due to the participation of $HO^{\bullet}$ radicals instead of h^+ in the reaction with
516 $O_2^{\bullet-}$ to form singlet oxygen. It can be concluded that this solar photocatalytic

517 TiO_2/graphene oxidation system can be a potential alternative to degrade wastewater
518 containing emerging contaminants, such as bisphenol-A.

519

520 **5. ACKNOWLEDGMENTS**

521 Financial support from MINECO (CTM2013-44317-R) is gratefully acknowledged.

522

6. REFERENCES

Akhavan, O, Ghaderi, E., 2009. Photocatalytic Reduction of Graphene Oxide Nanosheets on TiO_2 Thin Film for Photoinactivation of Bacteria in Solar Light Irradiation. J. Phys. Chem. C 113, 20214–20220.

Bellobono, I. R., Morazzoni, F., Bianchi, R., Mangone, E.S., Stanescu, R., Costache, C., Tozzi, P.M., 2005. Solar energy driven photocatalytic membrane modules for water reuse in agricultural and food industries. Pre-industrial experience using s-triazines as model molecules. Int. J. Photoenergy 7, 87-94.

Bielski, B.H.J., Cabelli, D.E., Arudi, R.L., Ross, A.B., 1985. Reactivity of $HO_2^{\bullet}/O_2^{\bullet-}$ Radicals in Aqueous Solution. J. Phys. Chem. Ref. Data 14, 1041-1100.

Crain, D.A. Eriksen, M., Iguchi, T., Jobling, S., Laufer, H., LeBlanc, G.A., Guillette, Jr. L.J., 2007. An ecological assesment of Bisphenol-A: Evidence from comparative biology. Reprod. Toxicol. 24, 225-239.

Daimon, T., Hirakawa, T., Kitazawa, M., Suetake, J., Nosaka, Y., 2008. Formation of singlet molecular oxygen associated with the formation of superoxide radicals in aqueous suspensions of TiO_2 photocatalysts. Appl. Catal. A: Gen. 340, 169-175.

544 Daneshvar, N., Rabbani, M., Modirshahla, N., Behnajady, M.A., 2004. Kinetic
545 modelling of photocatalytic degradation of Acid Red 27 in UV/TiO2 process. J.
546 Photoch. Photobio. A: 168, 39-45.

547

548 Durán, A., Monteagudo, J.M., San Martín, I., Sánchez-Romero, R., 2009. Photocatalytic
549 treatment of IGCC power station effluents in a UV-pilot plant. J. Hazard. Mater., 167,
550 885-891.

551

552 Esplugas, S., Bila, D.M., Krause, L.G.T., Dezotti, M., 2007. Ozonation and advanced
553 oxidation technologies to remove endocrine disrupting chemicals (EDCs) and
554 pharmaceuticals and personal care products (PPCPs) in water effluents. J. Hazard.
555 Mater., 149, 631-642.

556

557 Fujishima, A., Zhang, X., Tryk, D.A., 2008. TiO_2 photocatalysis and related surface
558 phenomena. Surf. Sci. Rep. 63, 515-582.

559

560 Fukahori, S., Ichiura, H., Kitaoka, T., Tanaka, H., 2003. Capturing of bisphenol A
561 photodecomposition intermediates by composite TiO_2 zeolite sheets. Appl. Catal.
562 B:Environ. 46, 453-462.

563

564 Gultekin, I., Mavrov, V., Ince, N.H., 2009. Degradation of Bisphenol-A by ozonation. J.
565 Adv. Oxid. Technol. 12, 242-248.

566

Hassan, F.M., Chabot, V., Li, J., Kim, B.K., Ricardez-Sandoval, L., Yu, A., 2013. Pyrrolic structure enriched nitrogen doped graphene for highly efficient next generation supercapacitors. J. Mater. Chem. A 1, 2904-2912.

Ho Y.S., McKay, G., 1999. Pseudo-Second Order Model for Sorption Processes. Process. Biochem. 34, 451-465.

Hu, J.Y., Chen, X., Tao, G., Kekred, K., 2007. Fate of endocrine disrupting compounds in membrane bioreactor systems. Environ. Sci. Tecnol. 41, 4097-4102.

Hummers, W.S., Offeman, R.E., 1958. Preparation of graphite oxide. J.Am. Chem. Soc. 80, 1339-1339.

Jin, Z., Wang, X., Sun, Y., Ai, Y., Wang, X., 2015. Adsorption of 4-n-Nonylphenol and Bisphenol-A on Magnetic Reduced Graphene Oxides: A Combined Experimental and Theoretical Studies. Environ. Sci. Technol. 49, 9168–9175.

Konstantinou, I.K., Albanis, T.A., 2003. TiO2-assisted photocatalytic degradation of azo dyes in aqueous solution: kinetic and mechanistic investigations. A review. Appl. Catal. B: Env. 49, 1-14.

Kumordzi, G., Malekshoar, G., Yanful, E. K., Ray, A. K., 2016. Solar photocatalytic degradation of Zn^{2+} using graphene based TiO_2. Sep. Purif. Technol. 168, 294-301.

590

591 Lagergren, S., 1898. Zur theorie der sogenannten adsorption gelöster stoffe. Kungliga
592 Svenska Vetenskapsakademiens, Handlingar 24, 1-39.

593

594 Lellala, K., Namratha, K. Byrappa, K., 2016. Ultrasonication assisted mild solvothermal
595 synthesis and morphology study of few-layered graphene by colloidal suspensions of
596 pristine graphene. Oxide Microp. Mesop. Mater. 226, 522-529.

597

598 Li, W., Zhao, S., Qi, B., Du, Y., Wang, X., Huo, M., 2009. Fast catalytic degradation of
599 organic dye with air and MoO3:Ce nanofibers under room condition. Appl. Catal. B:
600 Environ. 92, 333-340.

601

602 Liao, G., Zhu, D., Zheng, J., Yin, J., Lan, B., Li, L., 2016. Efficient mineralization of
603 bisphenol A by photocatalytic ozonation with TiO_2 –graphene hybrid. J. Taiwan Inst.
604 Chem. E. 67, 300-305.

605

606 Luoa, A., Yangb, Y., Zhanga, A., Wangd, M., Liud, Y., Biand, L., Jianga, F.,
607 PanbaKey, X., 2015. Hydrothermal synthesis of fluorinated anatase TiO_2/reduced
608 graphene oxide nanocomposites and their photocatalytic degradationof bisphenol A.
609 Appl. Surf. Sci. 353, 469-479.

610

611 Malekshoar, G., Pal, K., He, Q., Yu, A., Ray, A. K., 2014. Enhnaced Solar
612 photocatalytic degradation of phenol with coupled graphene-based titanium dioxide and
613 zinc oxide. Ind. Eng.Chem.Res. 53, 18824-18832.

614

615 Monteagudo, J.M., Durán, A., San Martin, I., Carnicer, A., 2011. Roles of different
616 intermediate active species in the mineralization reactions of phenolic pollutants under a
617 UV-A/C photo-Fenton process. Appl. Catal. B: Environ. 106, 242-249.

618

619 Muruganandham, M., Swaminathan, M., 2004. Solar photocatalytic degradation of a
620 reactive azo dye in TiO_2-suspension. Sol. Energy Mater. Sol. Cells 81, 439-457.

621

622 Ni, M., Leung, M.K.H., Leung, D.Y.C., Sumathy, K., 2007. A review and recent
623 developments in photocatalytic water-splitting using for hydrogen production. Renew.
624 Sustain. Energy Rev. 11, 401-425.

625

626 Patterson, A.L., 1939. The Scherrer Formula for X-Ray Particle Size Determination.
627 Phys. Rev. 56, 978- 982.

628

629 Pérez, M., Torrades, F., Domenech, X., Peral, J., 2002. Fenton and photo-Fenton
630 oxidation of textile effluents. Wat. Res. 36, 2703-2710.

631

632 Robert, D., Piscopo, A., Weber, J.V., 2004. Selective solar photodegradation of
633 organopollutant mixtures in water. Sol. Energy 77, 553-558.

634

635 Rogers, J.A., Metz, L., Yong, V.W., 2013. Review: Endocrine disrupting chemicals and
636 immune responses: A focus on Bisphenol-A and its potential mechanisms. Mol.
637 Immunol. 53, 421-430.

638

639 Rubin, B.S., 2011. Bisphenol-A: An endocrine disruptor with widespread exposure and
640 multiple effects. J. Steroid. Biochem. Mol. Biol. 127, 27-34.

641

642 Saha, S., Wang, J.M., Pal, A., 2012. Nano silver impregnation on commercial TiO_2 and
643 a comparative photocatalytic account to degrade malachite Green. Sep. Purif. Technol.
644 89, 147-159.

645

646 Sanchez-Polo, M., Abdel daiem, M.M., Ocampo−Perez, R., Rivera−Utrilla, J., Mota,
647 A.J., 2013. Comparative study of the photodegradation of Bisphenol A by $HO^{\bullet}$, $SO4^{\bullet-}$
648 and CO_3^{-}/HCO_3^{-} radicals in aqueous phase. Sci. Total Environ. 463−464, 423–431.

649

650 Saran M., Summer, K.H., 1999. Assaying for hydroxyl radicals: hydroxylated
651 terephthalate is a superior fluorescene marker than hydroxylated benzoate. Free Rad
652 Res. 31, 429-436.

653

654 Schafer, T.E., Lapp, C.A., Hanes, C.M., Lewis, J.B., Wataha, J.C., Schuster, G.S., 1999.
655 Estrogenicity of bisphenol A and bisphenol A dimethacrylate in vitro. J. Biomed. Mater.
656 Res. 45, 192-197.

657

658 Shen, Y., Fang, Q.L., Chen, B.L., 2014. Environmental applications of three-
659 dimensional graphene-based macrostructures: adsorption, transformation, and detection.
660 Environ. Sci. Technol. 49, 67–84.
661
662 Upadhyay, R.K., Soin, N., Roy, S.S., 2014. Role of graphene/metal oxide composites as
663 photocatalysts, adsorbents and disinfectants in water treatment: a review. RSC Adv. 4,
664 3823-3851.
665
666 Wang, R.C., Yu, C.W., 2013. Phenol degradation under visible light irradiation in the
667 continuous system of photocatalysis and sonolysis. Ultrason. Sonochem. 20, 553–564.
668
669 Xekoukoulotakis, N.P., Drosou, C., Brebou, C., Chatzisymeon, E., Hapeshi, E., Fatta-
670 Kassinos, D., Mantzavinos, D., 2011. Kinetics of UV-A/TiO_2 photocatalytic
671 degradation and mineralization of the antibiotic sulfamethoxazole in aqueous matrices.
672 Catal. Today, 161, 163-168.
673
674 Yanga, L., Lia, Z., Jianga, H., Jianga, W., Sua, R., Luoa, S., Luoa, Y., 2016.
675 Photoelectrocatalytic oxidation of bisphenol A over mesh of TiO_2/graphene/Cu_2O.
676 Appl. Catal. B:Environ. 183, 75-85.
677
678 Yoon, S.H., Jeong, S., Lee, S., 2012. Oxidation of Bisphenol A by UV/$S_2O_8^{2-}$: a
679 comparison with UV/H_2O_2. J. Environ. Technol. 33, 123–128.
680

Young, T., Geng, M., Thagard, C.A., 2013. Oxidative degradation of Bisphenol A: a comparison between Fenton reagent, UV, UV/H_2O_2 and Ultrasound. J. Adv. Oxid. Technol. 16, 89–101.

687 **Figure captions:**

688

689 **Figure 1**: a) Structure and properties of Bisphenol-A; b) Schematic illustration of the

690 experimental set-up.

691

692 Figure 2: Normalized UV–vis diffuse reflectance spectra (DRS) of TiO_2 and

693 TiO_2/graphene-2 wt% composite.

694

695 **Figure 3:** a) XRD pattern of TiO_2; b) XRD pattern of TiO_2/graphene; c,d) TEM images

696 of TiO_2/graphene nanocomposite; e) TEM images of graphene sheets; f) TEM images

697 of TiO_2 spheres.

698

699 **Figure 4**: a) Pseudo-first-order kinetics for the adsorption of BPA on TiO_2 surface; b)

700 Pseudo-first-order kinetics for the adsorption of BPA on TiO_2/graphene surface; c)

701 Pseudo-second-order kinetics for the adsorption of BPA on TiO_2 surface; d) Pseudo-

702 second-order kinetics for the adsorption of BPA on TiO_2/graphene surface.

703

704 **Figure 5:** a) Mineralization degree of BPA solutions under the TiO_2/graphene

705 photocatalyst with 1, 2 and 3 wt% of graphene. b) Effect of weight percentage of

706 graphene in the TiO_2/graphene composite on the pseudo-first-order kinetic rate constant.

707 Experimental conditions: [BPA]: 2.5 mg L^{-1}; **[**TiO_2]: 250 mg L^{-1}; solar power: 25-30

708 W/m^2; average temperature: 26ºC; reaction time: 120 min.

709

710 **Figure 6:** Evolution of the concentration of hydroxyl radicals and dissolved oxygen

711 along the BPA degradation reaction. a-b) solar/TiO_2 process: Influence of the initial

712 BPA concentration, **[**TiO_2]: 125 mg L^{-1}; c-d) solar/TiO_2 and solar/TiO_2/graphene

processes: Effect of TiO_2 loading, [BPA]: 5 mg L^{-1}. Solar power: 25-30 W/m^2; average temperature: 26ºC; reaction time: 120 min.

Figure 7: Roles played by different intermediate oxidative species in the degradation of BPA solutions under a) solar TiO_2 process; b) solar TiO_2/graphene process. Experimental conditions: [BPA]: 2.5 mg L^{-1}; **[**TiO_2/graphene]: 250 mg L^{-1}/2 %wt; solar power: 25-30 W/m^2; average temperature: 26ºC; reaction time: 120 min.

723 **Table 1. N_2 adsorption-desorption characteristics of pure TiO_2 P25 and**
724 **TiO_2/graphene-2 wt% composites**
725

Sample	Surface area[a] ($m^2\ g^{-1}$)	Pore volumen[b] ($cm^3\ g^{-1}$)	Average pore size[c] (nm)
TiO_2 P25	50.56	0.27	19.99
TiO_2/graphene	55.41	0.46	28.84

726 [a] BET specific surface area was calculated from the linear part of the corresponding
727 BET plot.
728 [b] BJH desorption cumulative pore volume between 1.7 and 300 nm diameters.
729 [c] Average pore diameter was estimated from the BJH formula
730
731
732
733
734
735 **Table 2. Kinetic parameters for the adsorption of BPA by TiO_2 or by**
736 **TiO_2/graphene**
737

Pseudo-second-order				
TiO_2			TiO_2/graphene	
	pH 2.5	pH 7.5	pH 2.5	pH 7.5
Q_e (mg/g)	18.149	18.248	31.056	31.056
k_2 (g min^{-1} mg^{-1})	0.0007	0.0037	0.0029	0.0043

738
739
740
741

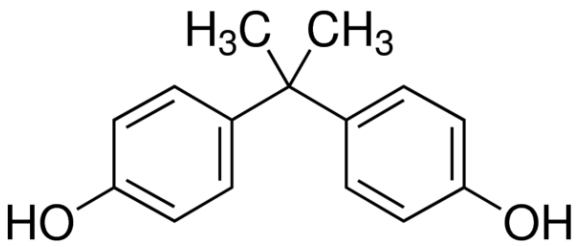

Linear formula: $(CH_3)_2C(C_6H_4OH)_2$

Molecular weight: 228.29 g mol^{-1}

Water solubility: 120 mg L^{-1} (25 ºC)

a)

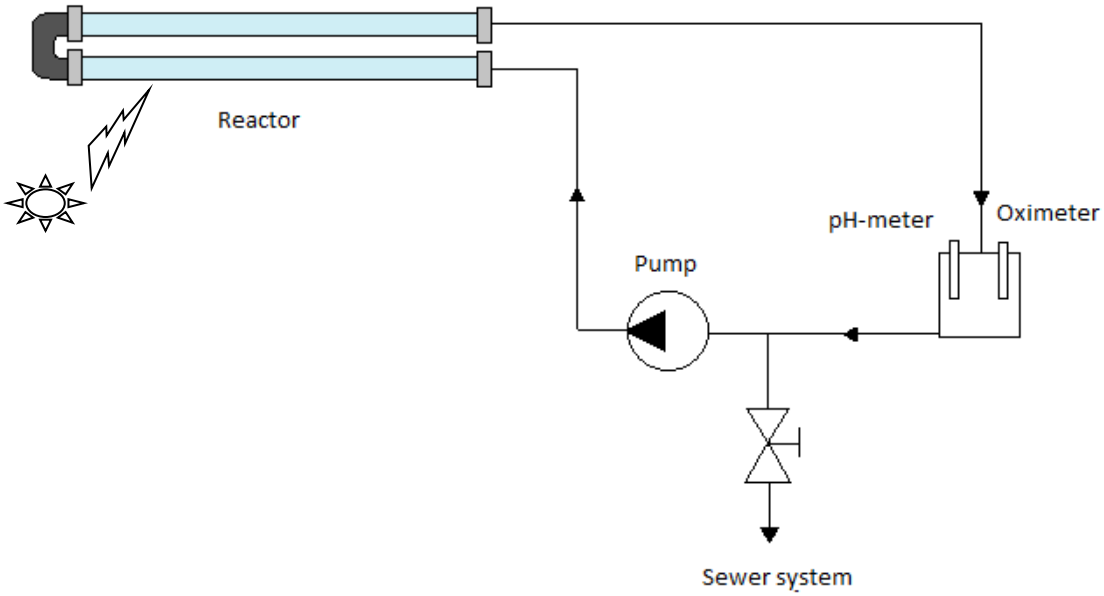

b)

Figure 1

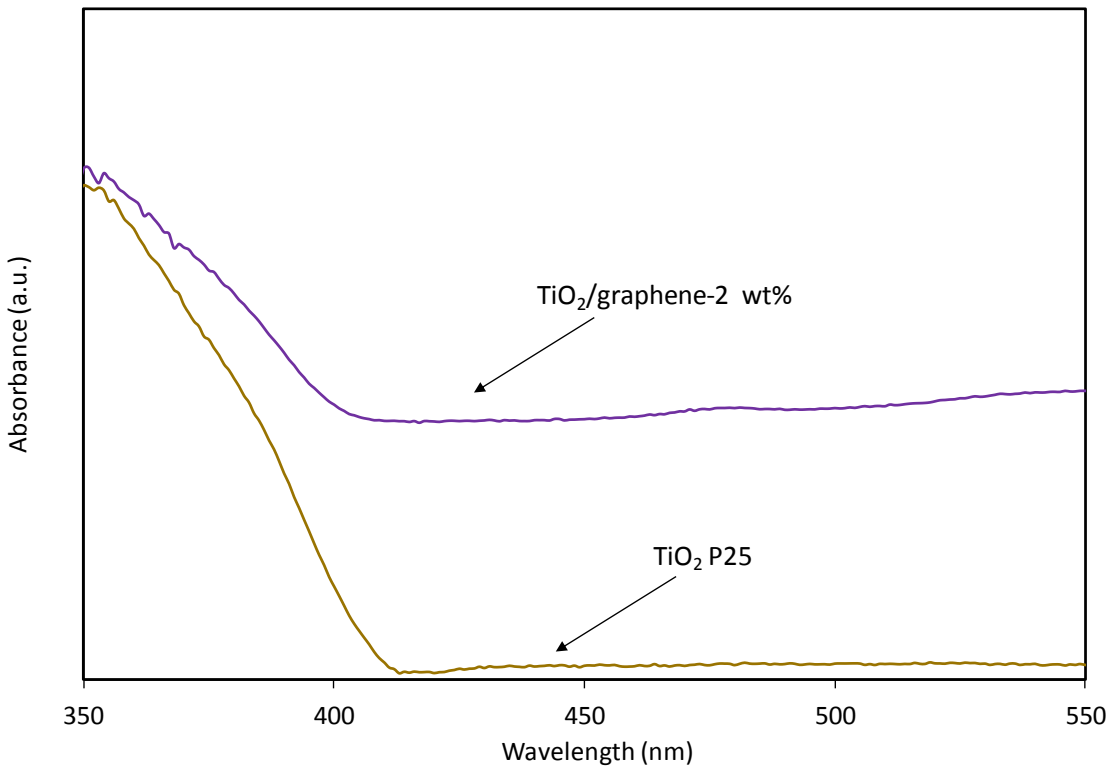
Absorbance (a.u.)
TiO2/graphene-2 wt%
TiO2 P25
350
400
450
500
550
Wavelength (nm)

Figure 2

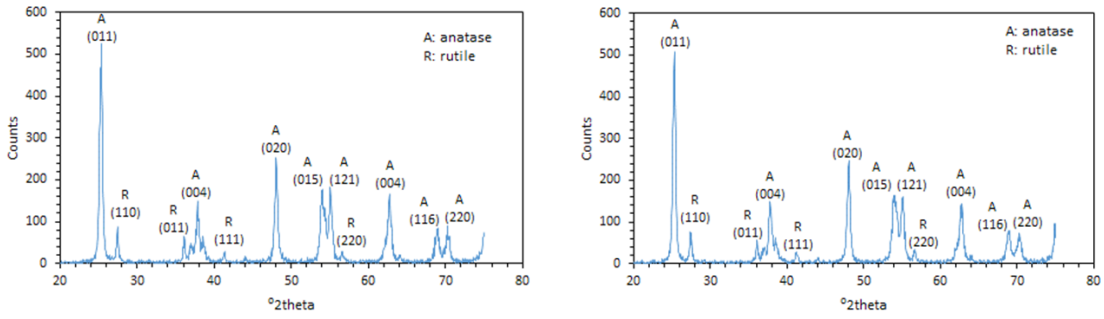

a) b)

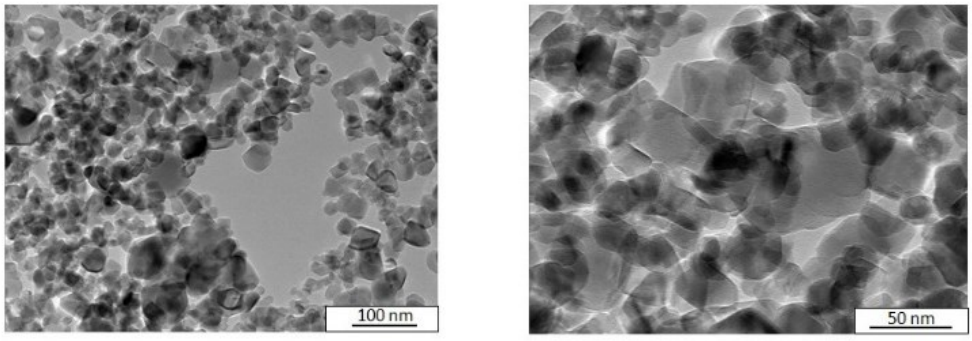

c) d)

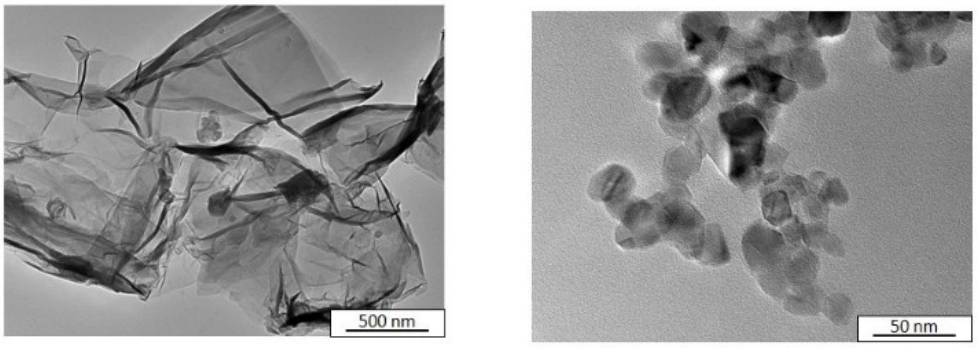

e) f)

Figure 3

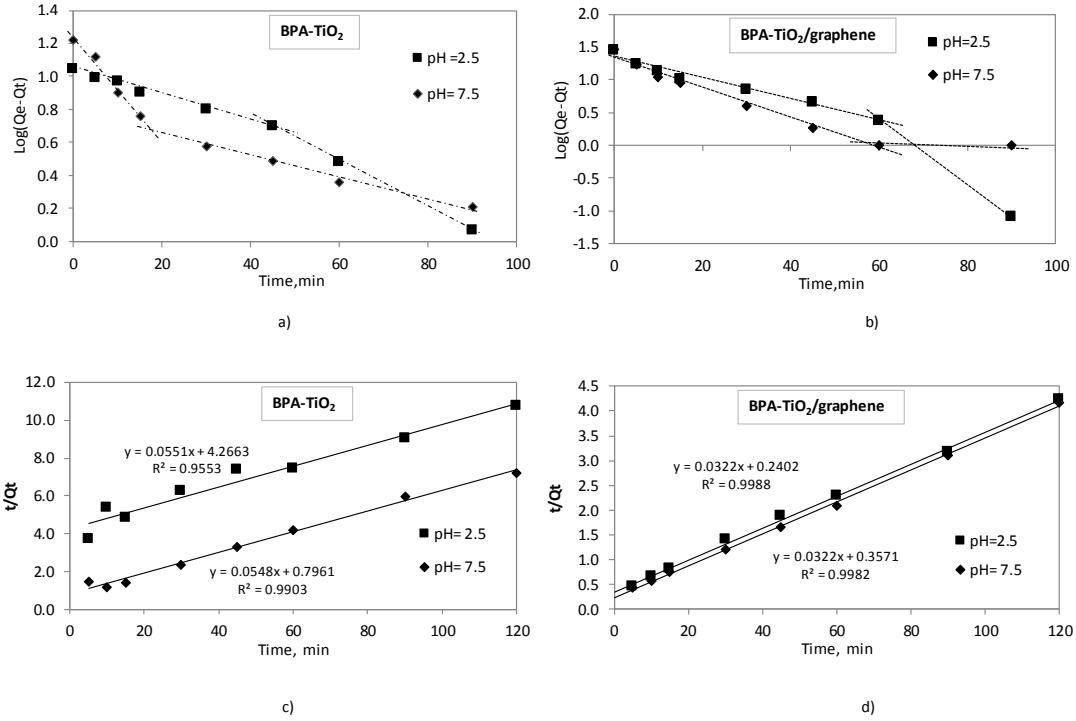

771

772 **Figure 4**

773

774

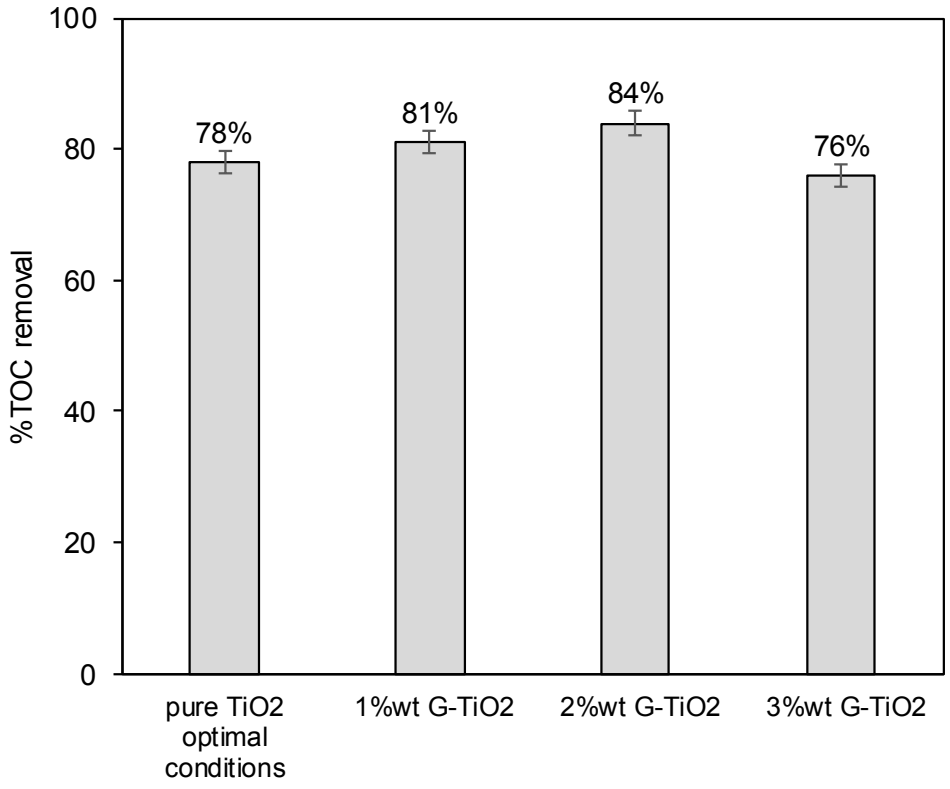
100
80
60
40
20
0
% TOC removal
78%
81%
84%
76%
pure TiO2 optimal conditions
1%wt G-TiO2
2%wt G-TiO2
3%wt G-TiO2

a)

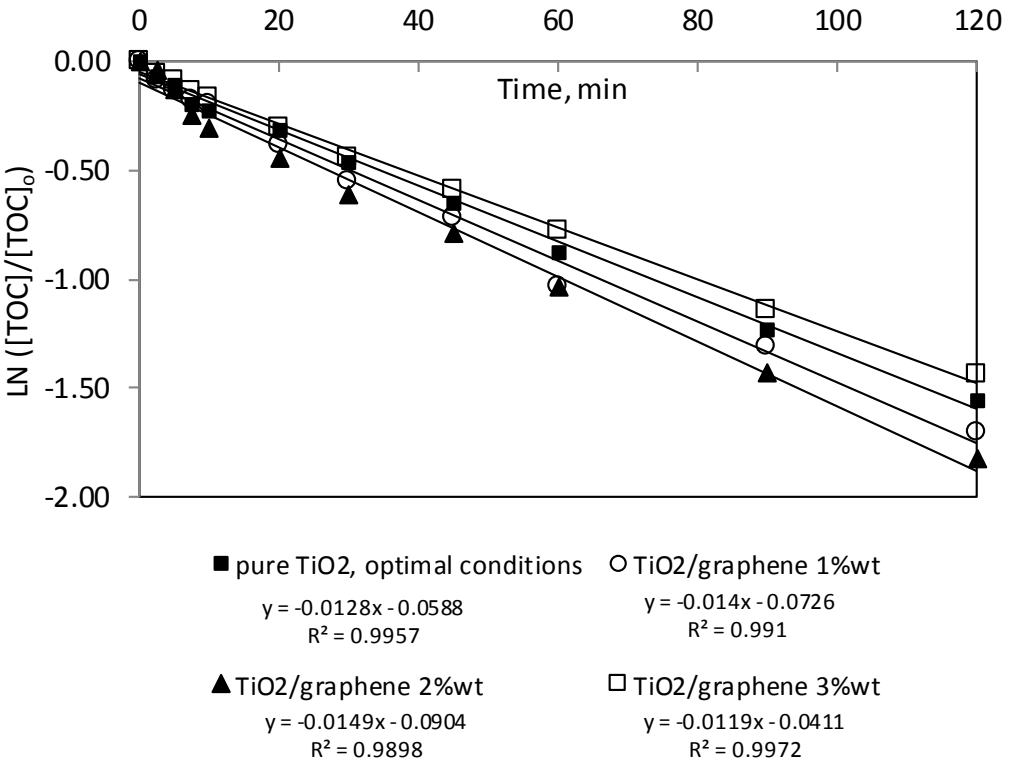
0
20
40
60
80
100
120
0.00
-0.50
-1.00
-1.50
-2.00
Time, min
LN ([TOC]/[TOC]o)
pure TiO2, optimal conditions
y = -0.0128x - 0.0588
R² = 0.9957
TiO2/graphene 1%wt
y = -0.014x - 0.0726
R² = 0.991
TiO2/graphene 2%wt
y = -0.0149x - 0.0904
R² = 0.9898
TiO2/graphene 3%wt
y = -0.0119x - 0.0411
R² = 0.9972

b)

775

776 **Figure 5**

777

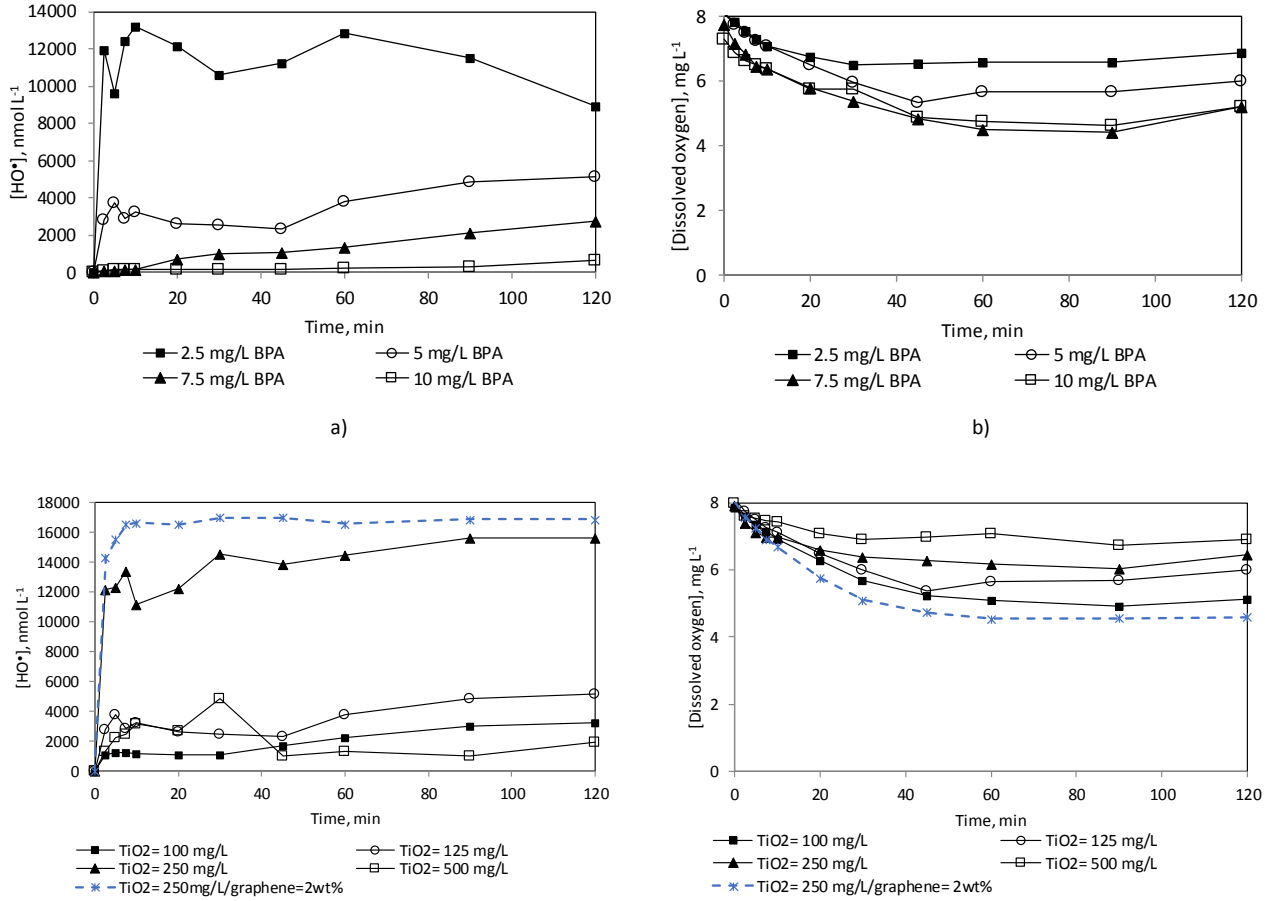

778

779 **Figure 6**

780

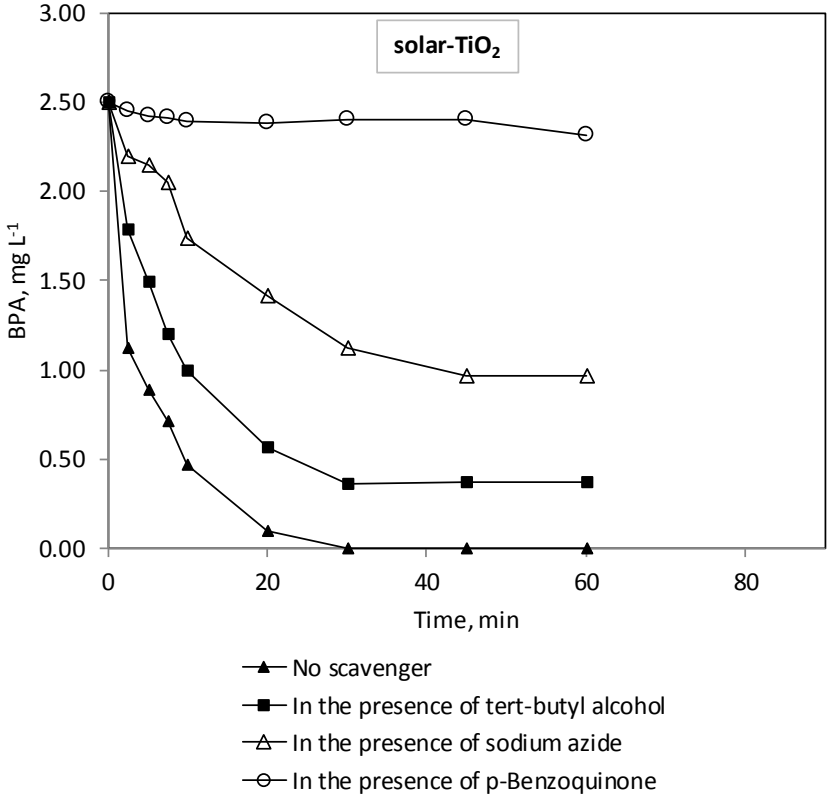
solar-TiO2
BPA, mg L-1
Time, min
No scavenger
In the presence of tert-butyl alcohol
In the presence of sodium azide
In the presence of p-Benzoquinone

a)

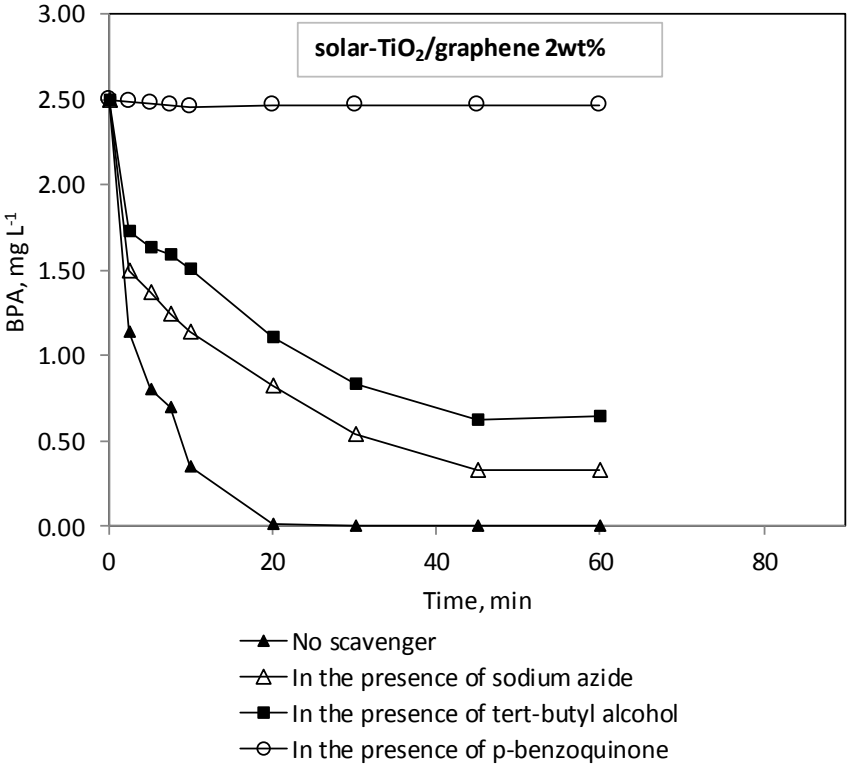
solar-TiO2/graphene 2wt%
BPA, mg L-1
Time, min
No scavenger
In the presence of sodium azide
In the presence of tert-butyl alcohol
In the presence of p-benzoquinone

b)

781

782 **Figure 7**